THREE-DIMENSIONAL SIMULATIONS OF PROTOSTELLAR JETS IN STRATIFIED AMBIENT MEDIA

ELISABETE M. DE GOUVEIA DAL PINO

Universidade de São Paulo, Instituto Astronômico e Geofisico, Avenida Miguel Stéfano 4200, São Paulo, SP 04301-901, Brazil; dalpino@astro1.iagusp.usp.br

AND

MARK BIRKINSHAW

Department of Physics, University of Bristol, Tyndall Avenue, Bristol BS8 1TL, England

ABSTRACT

We present fully three-dimensional hydrodynamic simulations of radiative cooling jets propagating into stratified isothermal ambient media with power-law density and pressure distributions. The parameters used are mainly suitable for protostellar jets, but results applicable to extragalactic jets are also presented. Comparisons are made with previous simulations of jets through homogeneous media. We find that, for radiative cooling jets propagating into regions where the ambient medium has an increasing density (and pressure) gradient, the ambient gas tends to compress the cold, low-pressure cocoon of shocked material that surrounds the beam and destroy the bow shock–like structure at the head. The compressing medium collimates the jet and promotes the development of Kelvin-Helmholtz instabilities, which cause beam focusing, wiggling, and the formation of internal traveling shocks, *close to the head,* via pinching along the beam. This remarkably resembles the structure of some observed systems (e.g., the Haro 6-5B northern and HH 24G jets). These effects are larger for jets with a smaller density ratio η between jet and environment (tested for $\eta = 1$, 3, and 10) and larger Mach numbers $M_a = v_j/c_a$ (tested for $M_a = 12$ and 24, where v_j is the jet velocity and c_a is the ambient sound speed). In an ambient medium of decreasing density (and pressure), the beam is poorly collimated and relaxes, becoming faint. This could explain "invisible" jet sections, like the gap between the parent source and collimated beam (e.g., in the HH 30 jet). Although, on average, jets propagating into an increasing (decreasing) density environment are decelerated (accelerated) by the increasing (decreasing) ram pressure of the ambient medium, we find that their propagation velocities have an oscillatory pattern. The internal traveling shocks that develop in jets propagating into positive density gradient environments display a similar velocity variation, in qualitative agreement with recent measurements of fluctuations in the tangential velocity of the knots of the Haro 6-5B jet. Finally, runs of adiabatic jets into similar stratified environments indicate that they are less affected by the effects of stratification than the cooling jets because their higher pressure cocoons are better able to preserve the beam structure.

Subject headings: hydrodynamics — ISM: jets and outflow — shock waves — stars: pre–main-sequence

1. INTRODUCTION

Supersonic jets emanating from protostars and active galactic nuclei propagate into complex media. Protostellar jets, for example, are immersed in molecular clouds that are composed of many smaller, dense clouds (see, e.g., Mundt, Ray, & Raga 1991, hereafter MRR; Bally & Devine 1994). Examining a sample of 15 protostellar jets, MRR found that the flows are often poorly collimated close to the source and become better collimated at large distances from their sources. The Haro 6-5B jet, in particular, after a section of strong expansion, narrows with increasing distance from the source, presumably because of reconfinement. These observations suggest that, in addition to some local collimation near the source, a very large scale collimation mechanism is at work, which is possibly due to the jet's external environment (MRR).

The question of what happens to radio-emitting extragalactic jets propagating into a nonhomogeneous medium was discussed by Sanders (1983), Falle & Wilson (1985a, 1985b), Wiita, Rosen, & Norman (1990), and Hardee et al. (1992), who performed two-dimensional hydrodynamic simulations of adiabatic, light jets. Since the radiative cooling distance behind the postshock gas in protostellar jets is smaller than the jet radius, an adiabatic approach is

inappropriate. Furthermore, the lack of backflowing cocoons associated with protostellar jets and the large advance speeds of their working surfaces suggest that they are usually denser than their surroundings. Earlier numerical modeling of jets emanating from protostars was performed for beams propagating into homogeneous ambient media (e.g., Blondin, Fryxell, & Königl 1990, hereafter BFK; de Gouveia Dal Pino & Benz 1993 [hereafter GB93], 1994 [hereafter GB94]; Chernin et al. 1994, hereafter CMGB; Stone & Norman 1993b [hereafter SN], 1994a, 1994b; Biro & Raga 1994). In this work, we examine the effects of stratified environments on the structure of radiatively cooling and adiabatic, initially heavy jets with the aid of three-dimensional numerical simulations using the smoothed particle hydrodynamics technique (see, e.g., GB93). Some of the results of these simulations and their possible correlation with observed wiggling jets have been recently summarized in de Gouveia Dal Pino, Birkinshaw, & Benz (1996, hereafter GBB). We here describe in more detail the results for a range of environmental and jet parameters.

Previous work on jets propagating into homogeneous ambient media has demonstrated that internal traveling knots may be produced by small-period velocity variations

in the ejection of the jet (e.g., Raga et al. 1990; Raga & Kofman 1992; Kofman & Raga 1992; Hartigan & Raymond 1992; GB94; SN). This mechanism favors the formation of knots closer to the driving source that become fainter and disappear at larger distances, as, for example, in jet systems like HH 34 and HH 111. In the present work, we find that the propagation of a radiative cooling jet into an atmosphere of increasing density (pressure) may drive the formation of internal knots closer to the jet head. This seems to be the case, for example, for the Haro 6-5B northern and HH 24G jets.

The organization of this work is as follows: In § 2, based on simple one-dimensional arguments, we discuss the basic theoretical properties of jets propagating into stratified ambient media and describe the assumptions of our numerical model, including the initial and boundary conditions, and the model parameters adopted for the simulations. In § 3, we present the results of our hydrodynamic simulations for jets propagating into stratified ambient media with positive and negative density gradients and different values of the density ratio between jet and ambient material, η, and of the Mach number, M_a. Finally, in § 4 we summarize our results and discuss their possible applications to observed protostellar jets.

2. DESCRIPTION OF THE MODEL

2.1. *Theoretical Grounds*

The basic properties of jets propagating into homogeneous ambient media are described in BFK and GB93. Similarly to Hardee et al. (1992), we assume an initial isothermal ambient medium ($T_a = 10^4$ K) with density (and pressure) distribution stratified along the jet axis x:

$$n_a(x) = n_a(x_0)F(x) , \tag{1}$$

where

$$F(x) = [\alpha(x - x_0) + 1]^\beta \tag{2}$$

and n_a is the number density, x_0 is the value of x at the jet inlet (in units of R_j, the jet radius), α is a dimensionless parameter of the model, and the exponent $\beta = \pm 5/3$ for positive and negative density gradients, respectively. Such profiles were chosen for compatibility with previous simulations of jets propagating into homogeneous environments. They are also consistent with the observed density distributions of the clouds that involve protostars (e.g., Fuller & Myers 1992). While a negative density gradient may represent, for example, the atmosphere that a jet encounters when it emerges from the protostar and propagates through the cloud that envelops the parent source, a positive density gradient may occur when a fully emerged jet enters an external cloud (GBB) since the density of the cloud increases as the jet submerges. In the simulations, the atmosphere was held steady by an appropriate gravitational potential, whose effects on the jet dynamics are negligible since the jets are assumed to be highly supersonic.

A supersonic jet propagating into a stratified ambient gas will develop a shock pattern at its head whose structure and strength will depend on the ambient density profile. The impacted ambient material is accelerated by a forward bow shock, whose velocity estimated from momentum flux conservation in one-dimensional analysis is approximately given by

$$v_{bs} \approx \frac{v_j}{1 + (\epsilon\eta)^{-1/2}F(x)^{1/2}} , \tag{3}$$

and the jet material is decelerated at the jet shock with a velocity $v_{js} \approx v_j - v_{bs}$. In the equation above, $\eta = n_j(x_0)/n_a(x_0)$ is the ratio between the jet and ambient number densities at the jet inlet ($x = x_0$), and $\epsilon^{1/2} = R_j/R_h$ is the ratio of jet to head radius. For a homogeneous ambient medium, for which $F(x) = 1$, equation (3) becomes identical to equation (2) of GB93. As long as ϵ remains constant, equation (3) predicts a global acceleration (deceleration) of the head of a $\eta > 1$ jet propagating into a negative (positive) density gradient ambient medium.[1]

For shock velocities $v_s > 90$ km s^{-1}, the cooling length in the postshock gas behind the shock is given, in units of the jet radius, by

$$q_s \equiv \frac{d_{cool}}{R_j} \approx 8 \times 10^{16} R_j^{-1} v_{s,7}^4 n^{-1} \tag{4}$$

(see, e.g., BFK), where n is the preshock number density (we have assumed a number density of nuclei $\approx n/2$) and $v_{s,7} = v_s/(10^7$ cm s^{-1}). Using equations (2) and (3) above, the cooling parameter for the bow shock is

$$q_{bs} \equiv \frac{d_{cool}}{R_j} \approx 8 \times 10^{16} R_j^{-1} v_{j,7}^4 n_a(x_0)^{-1}$$
$$\times \frac{F(x)^{-1}}{[1 + (\epsilon\eta)^{-1/2}F(x)^{1/2}]^4} , \tag{5}$$

and the cooling parameter for the jet shock is

$$q_{js} \approx q_{bs}\epsilon^{-2}\eta^{-3}F(x)^3 . \tag{6}$$

Equations (3), (5), and (6) indicate that, as long as ϵ remains unaltered and $\eta > 1$, as the jet propagates downstream into an ambient medium with negative density gradient [decreasing $F(x)$], the gas behind the bow shock will become increasingly adiabatic (q_{bs} increases) while the jet shock will become increasingly radiative (q_{js} decreases with increasing v_{bs} and, hence, decreasing v_{js}). The reverse situation must hold for jet propagation into an ambient medium with positive density gradient.

We note that, for example, in an ambient medium with negative density gradient, as v_{js} decreases with increasing v_{bs}, it may eventually become smaller than 90 km s^{-1}. In such a case, q_{js} is more correctly evaluated through

$$q_{js} \simeq 0.31\left(\frac{n_j}{1000 \text{ cm}^{-3}}\right)^{-1}$$
$$\times \left(\frac{v_{js}}{45 \text{ km s}^{-1}}\right)^{-4.7}\left(\frac{R_j}{2 \times 10^{16} \text{ cm}}\right)^{-1} \tag{7}$$

(see, e.g., Falle & Raga 1993), where n_j is the jet number density.

The density n_{sh} of the cold shell that develops in the working surface from the radiative cooling of the shocked gas can be estimated by balancing the ram pressure of the ambient medium and the thermal pressure of the cooled

---

[1] However, the numerical simulations below show that v_{bs} often develops an oscillatory pattern caused by the combined effects of ϵ and the ambient ram pressure ($n_a v_{bs}^2$) variations; see § 4.

gas:

$$n_{\rm sh} K T_{\rm sh} \approx \bar{m} n_a(x_0) v_j^2 \frac{F(x)}{[1 + (\epsilon\eta)^{-1/2} F(x)^{1/2}]^2} . \qquad (8)$$

The right-hand side gives the ambient ram pressure ($\rho_a v_{\rm bs}^2$), K is the Boltzmann constant, and $\bar{m}$ is the mean mass per particle, which is constant in the case of complete ionization. Therefore, for a jet propagating downstream into a positive density gradient atmosphere, $n_{\rm sh}$ will increase for an $\eta > 1$ jet ($\epsilon \sim$ constant) as long as $(\epsilon\eta)^{-1/2} F(x)^{1/2}$ remains less than 1. However, as $F(x)$ becomes very large, $n_{\rm sh}$ will tend to an approximately constant value [$n_{\rm sh} \approx \bar{m} n_a(x_0) v_j^2 \eta / K T_{\rm sh} \epsilon$].

We note that equations (4)–(8) above apply only in the region close to the axis of symmetry of the jet, as pressure gradient effects must be nonnegligible off the axis. Nonetheless, § 3 below indicates that the predictions of the one-dimensional relations above are qualitatively supported by the three-dimensional simulations.

2.2. The Numerical Model

The hydrodynamics equations are solved by using a modified version of the three-dimensional, gridless, Lagrangian smoothed particle hydrodynamics (SPH) code described in Benz (1990), GB93, GB94, and CMGB. The ambient gas is represented by a three-dimensional rectangular box filled with particles. A supersonic jet of radius R_j is injected continuously into the bottom of the box, which has dimensions up to $\sim 30R_j$ in the x-axis and $12R_j$ in the transverse directions y and z. All distances are normalized to the jet radius. The boundaries of the box are assumed to be continuous ($\partial v = 0$)—particles are removed from the system whenever they cross the boundaries. (In the original code [GB93], the transverse boundaries were assumed to be periodic. With the present modification to continuous boundaries, the formation of undesirable reflective waves on the transverse boundaries, later in the simulations, is prevented.) The SPH particles are smoothed out in space with a spherically symmetric kernel function of initial width 0.4 or 0.5 and 0.2 or 0.25 times R_j for the ambient and jet particles, respectively.

As in the previous works (GB93, GB94; CMGB), the jet and the ambient gas are treated as a single ionized fluid with a ratio of specific heats $\gamma = 5/3$ and an ideal gas equation of state $p = u(\gamma - 1)\rho$, where u is the internal energy per unit mass, p is the thermal pressure, and $\rho = n\bar{m}$ is the mass density.

The radiative cooling (due to collisional excitation and de-excitation, and recombination) is calculated by using the cooling function evaluated by Katz (1989) for a gas of cosmic abundances cooling from $T = 10^6$ K. The cooling is suppressed below $T \approx 10^4$ K, when the assumption of completely ionized flow breaks down and the effects of transfer of ionizing radiation become important. A time-implicit scheme combined with Newton-Raphson (NR) iterations is used to evolve the cooling rate. To monitor accuracy, the maximum change in a time step is kept less than 30%. If this condition is not achieved, or if the system fails to converge in 100 NR iterations, the time step is reduced (to $\Delta t/2$) and a solution is once again pursued. The limitations of the cooling assumptions are discussed in GB93 and GB94. By not taking into account the effects of nonequilibrium ionization of the gas or the transfer of ionizing radiation, we are probably underestimating the cooling rate in some parts

of the postshock regions by as much as an order of magnitude (see, e.g., Innes, Giddings, & Falle 1987). However, a comparison of our results (see also GB93) with multidimensional calculations for steady flows in a homogeneous ambient medium, which have included a nonequilibrium time-dependent cooling (SN), show that the essential dynamical features do not change significantly under the presence of nonequilibrium ionization effects.

The evolution of the system is parameterized by the dimensionless numbers (1) $\eta = n_j/n_a$ (the ratio between the input jet and ambient number densities at x_0; eq. [2]); (2) $M_a = v_j/c_a$ [the initial ambient Mach number, where the ambient sound speed is given by $c_a = (\gamma k T_a/\bar{m})^{1/2}$, with T_a being the ambient temperature (held constant even in stratified atmospheres) and $\bar{m} \simeq 0.5m_{\rm H}$ the mean mass per particle for a fully ionized gas of cosmic abundances]; (3) $k_p = p_j/p_a$ (the input pressure ratio, which has been assumed to be initially equal to unity in all simulations); and (4) $q_{\rm bs}(0)$ (eq. [5]). The stratification of the ambient medium described by equations (1) and (2) adds two new parameters to the models, α and β.

Based on typical conditions found in protostellar jets, the parameters of the simulations were chosen to be the following: density ratio $\eta \simeq 1$–10 (see, e.g., Mundt, Brügel, & Bührke 1987; Morse et al. 1992; Raga & Noriega-Crespo 1993); ambient number density $n_a(0) \simeq 200$ cm^{-3}; jet velocities $v_j \simeq 200, 400$ km s^{-1} (see, e.g., Reipurth 1989a; Reipurth, Raga, & Heathcote 1992); initial ambient Mach numbers $M_a = 12, 24$; and jet radius $R_j = 2 \times 10^{15}$ cm (see, e.g., Raga 1993). For the parameters of the stratified ambient medium (eqs. [1] and [2]), we assume $\alpha = 0$–0.5 and $\beta = \pm 5/3$. We note that the values adopted for α and β correspond to large pressure and density gradients, which allow us to investigate structural effects on the simulated beams without having to make them propagate too many jet radii. In fact, large gradients do exist in the ISM through which the jets propagate, as we have remarked in § 1, and the evolution of these gradients with time is much slower than the evolution of the jet structures, so the assumption of a nearly steady atmosphere is reasonable.

The limitations to our SPH simulations are discussed in GB93, GB94, and CMGB; in particular, we remark that turbulence, which is active in these flows since the Reynolds numbers are very high, greater than 10^4 (GB93), is difficult to study because our initial particle spacing is quite large relative to the size of eddies that may develop in the flow and because the numerical viscosity of the code may be too dissipative. Thus, for this work, we can only consider the bulk properties of the flow, i.e., over a size scale larger than that of most of the largest eddies, at which the internal turbulent motions are averaged out.

3. THE SIMULATIONS

We have performed runs of radiative cooling supersonic jets using different values of η, M_a, and the α- and β-parameters for the stratified ambient medium. The effects of stratification on adiabatic jets were also examined. The subsections below present the results of these calculations, and Table 1 summarizes the values of the input parameters of our simulations.

3.1. Effects of Ambient Media with Different (α, β)

Figure 1 depicts the central density contours and the velocity distribution of five cooling jets at a time $t = 0.85$ (in

TABLE 1
VALUES OF THE INPUT PARAMETERS OF OUR MODELS

Figure	α	β	η	M_a	$q_{bs}(x_0)$	$q_{js}(x_0)$
1a	0.5	5/3	3	24	8.1	0.3
1b	0.1	5/3	3	24	8.1	0.3
1c	0	0	3	24	8.1	0.3
1d	0.1	−5/3	3	24	8.1	0.3
1e	0.5	−5/3	3	24	8.1	0.3
2, 5 (top)	0	0	3	24	8.1	0.3
3, 5 (center)	0.5	5/3	3	24	8.1	0.3
4, 5 (bottom)	0.5	−5/3	3	24	8.1	0.3
7a, 8	0.5	5/3	1	24	3.1	3.1
7b	0.5	5/3	3	24	8.1	0.3
7c	0.5	5/3	10	24	16.7	0.008
9a	0.5	−5/3	1	24	3.1	3.1
9b	0.5	−5/3	3	24	8.1	0.3
9c	0.5	−5/3	10	24	16.7	0.008
10	0.5	5/3	3	12	0.5	0.019
11	0.5	−5/3	3	12	0.5	0.019
12	0.5	5/3	3	24	0	0
13	0.5	−5/3	3	24	0	0

units of $t_{ja} = R_j/c_a = 38.2$ yr) evolving through ambient media with positive density stratification (Figs. 1a, 1b); no stratification (Fig. 1c); and negative density stratification (Figs. 1d, 1e) (see Table 1). All the jets have the initial conditions $\eta = 3$, $n_a(x_0) = 200$ cm^{-3}, $R_j = 2 \times 10^{15}$ cm, $v_j = 398$ km s^{-1}, $M_a = 24$, $q_{bs}(x_0) \approx 8.1$ (corresponding to an initial bow shock velocity $v_{bs} \approx 252$ km s^{-1}), and $q_{js}(x_0) \approx 0.3$ (corresponding to an initial jet shock velocity $v_{js} \approx 146$ km s^{-1}). The maximum density reached by the cold shell that develops at the head of the jet from the cooling of the shock-heated gas, $n_{sh}/n_a(x_0)$, is in rough agreement with equation (8). We clearly see an acceleration of the jet due to the decrease of the ambient density and ram pressure ($n_a v_{bs}^2$) from Figures 1a–1e. Consistent with equation (3), the propagation velocity of the beam, v_{bs}, increases with increasing η.

Figures 2, 3, and 4 compare the density and velocity evolution of three cases with $\eta = 3$. In Figure 2, the ambient medium is homogeneous ($\alpha = 0$, $\beta = 0$); in Figure 3, the ambient medium has a positive density gradient ($\alpha = 0.5$, $\beta = 5/3$); and in Figure 4, it has a negative density gradient ($\alpha = 0.5$, $\beta = -5/3$). The initial conditions are the same as in Figure 1.

In the homogeneous medium (Fig. 2), we identify the same features detected in previous works (e.g., BFK; SN; GB93, GB94; CMGB). At the head of the jet, a dense shell of shocked jet material develops. It becomes Rayleigh-Taylor (GB93) unstable and breaks into blobs. The density of the shell also undergoes variations with time as a result of global thermal instabilities of the radiative shock (see GB93 for details). A thin, low-density cocoon containing postshock jet gas is deposited around the beam. A shroud of shocked ambient gas envelops both the beam and the cocoon.

In the increasing-density (and pressure) medium (Fig. 3), the cocoon/shroud is compressed and pushed backward by the increasing ram pressure of the ambient medium (see also GBB). An elongated structure (Figs. 3c, 3d) replaces the bow shock seen in front of the head of the jet propagating into the uniform medium of Figure 2. The increasing pressure and density of the surrounding medium collimate the beam and promote the development of the Kelvin-Helmholtz (K-H) instability (see, e.g., Birkinshaw 1991), and the inherent

discreteness of the SPH code in the beam excites pinch and helical modes (Fig. 3c). These modes overconfine the beam, drive internal shocks, and cause some jet wiggling (see also Figs. 7a, 7b, and 8 below). It is interesting to note that this beam structure is similar to the one found for adiabatic jets propagating into a homogeneous ambient medium (GB93). In the latter cases, however, the collimation of the beam is a result of the hot, high-pressure postshock jet gas in the cocoon immediately behind the working surface.

On average, jets propagating into an ambient medium of increasing density gradient are decelerated by the increasing ambient ram pressure ($n_a v_{bs}^2$). However, for the jet of Figure 3 (see also Figs. 7 and 8 below), we find that the propagation velocity, v_{bs}, has an oscillatory pattern caused by competition between the $F(x)$ and $\epsilon(x)$ terms in equation (3). Since $F(x)$ increases with distance, v_{bs} initially decreases as the jet propagates downstream with $\epsilon^{1/2} \approx 1$. As the jet head is compressed by the ambient medium, however, the increase of ϵ more than compensates for the decrease of $F(x)$, and the jet head accelerates as it narrows. Eventually, the further decrease of $F(x)$ again dominates, and the working surface decelerates again. Table 2 shows the velocity variations in the head of the jet of Figure 3 as a function of time and the position of the bow shock ($x_{bs} - x_0$) (see also GBB). The varying bow shock and jet shock velocity ($v_{js} \approx v_j - v_{bs}$) may cause the ambient ram pressure ($n_a v_{bs}^2$; Table 2) and the radiative cooling distances behind both shocks, q_{bs} and q_{js}, to fluctuate (eqs. [5] and [6]) and the working surface to become thermally unstable (GB93). On average, however, the bow shock becomes more radiative and the jet shock more adiabatic as the jet propagates downstream, in qualitative agreement with equations (5), (6), and (7). Following the oscillatory pattern, the maximum density in the shell at the head $n_{sh}/n_a(x_0)$ varies from ≈ 847 ($t/t_{ja} = 0.85$) to 3550 ($t/t_{ja} = 1.25$), 651 ($t/t_{ja} = 1.65$), and 741 ($t/t_{ja} = 1.95$), in Figures 3a, 3b, 3c, and 3d, respectively. The internal shocks of the beam have peak separations $\sim(1 - 2)R_j$ and travel downstream with a similar variable velocity as the working surface. The shocks closer to the jet head have their speed closer to v_{bs}.

In the decreasing-density (and pressure) medium (Fig. 4), the jet retains a well-developed bow shock and cavity structure. The beam shows a slight decollimation close to the head ($\epsilon^{1/2} \approx 0.7$ in the bottom two rows of Fig. 4; see also Fig. 9 below). On average, it propagates downstream with increasing velocity ($v_{bs} \approx 285$, 325, 353, and 376 km s^{-1} from top to bottom in Fig. 4), as a result of the declining ambient ram pressure, in rough agreement with equations (1), (2), and (3). The cold shell at the head is thin and without

TABLE 2
VELOCITY OSCILLATIONS IN THE HEAD OF THE $\eta = 3$ JET PROPAGATING INTO AN ENVIRONMENT OF INCREASING DENSITY[a]

t/t_{ja}	$(x_{bs} - x_0)/R_j$	$\epsilon^{1/2}$	v_{bs} (km s^{-1})	$n_a v_{bs}^2$ [b]
0	0	1	250	2.3×10^2
0.45	5.3	1.2	200	1.2×10^3
0.85	8.8	1.4	144	1.2×10^3
1.25	12	1.6	130	1.7×10^3
1.65	18.7	3.3	260	1.2×10^4
1.95	23	3.2	225	1.2×10^4

[a] As shown in Figs. 3 and 7b ($\alpha = 0.5$, $\beta = 5/3$).
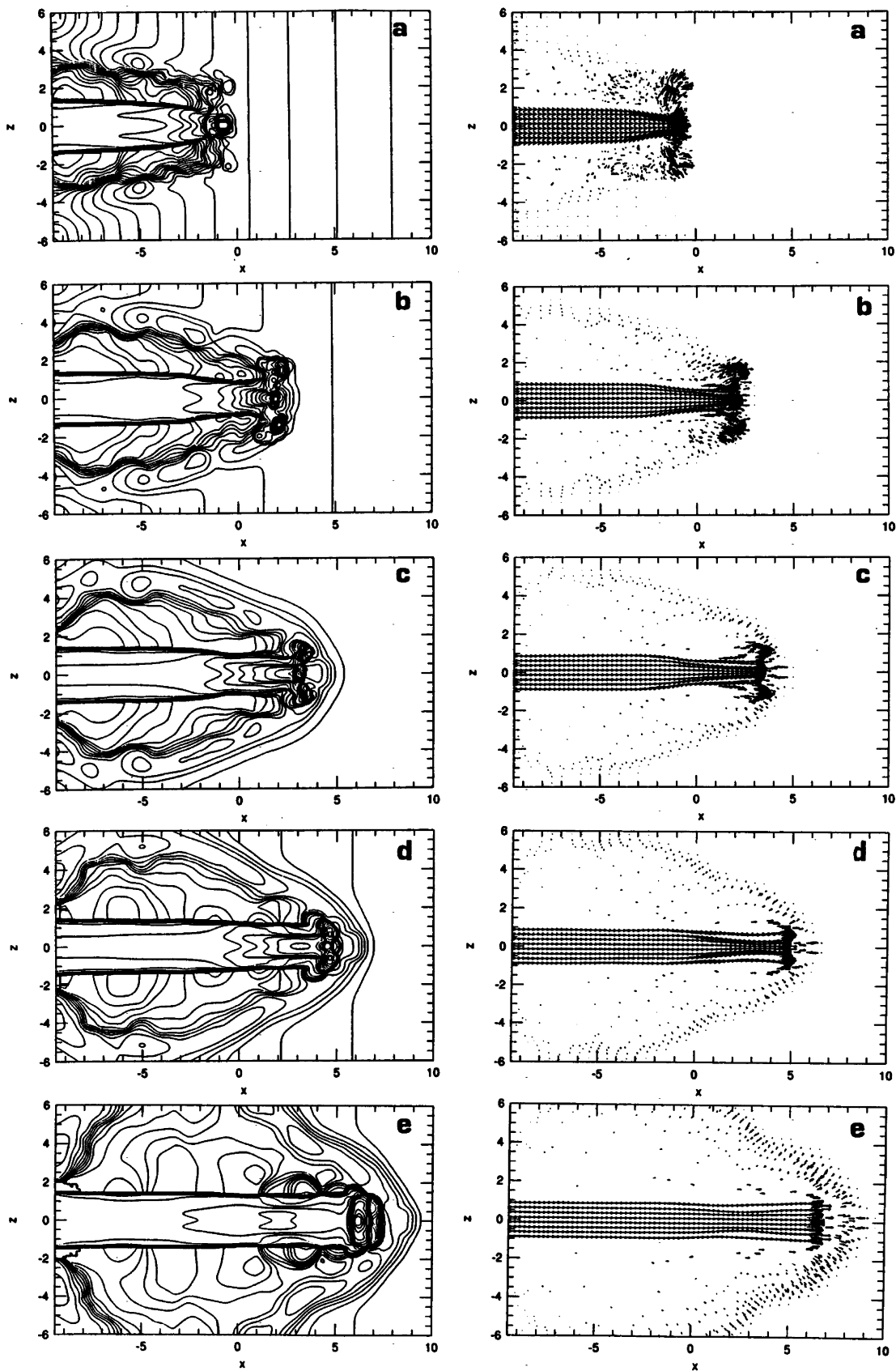[b] In units of $n_a(x_0)c_a^2 = 5.5 \times 10^{14}$ cm^{-1} s^{-2}.

Fig. 1.—Midplane density contours (*left*) and velocity distribution (*right*) of five radiative cooling jets at $t = 0.85 \, R_j/c_a$ (=38.2 yr) evolving through different stratified ambient media with (*a*) $\alpha = 0.5$, $\beta = 5/3$, (*b*) $\alpha = 0.1$, $\beta = 5/3$, (*c*) $\alpha = 0$, $\beta = 0$, (*d*) $\alpha = 0.1$, $\beta = -5/3$, and (*e*) $\alpha = 0.5$, $\beta = -5/3$. The initial parameters are $\eta = 3$, $n_a = 200 \, \text{cm}^{-3}$, $R_j = 2 \times 10^{15}$ cm, $M_a = 24$, and $v_j = 398$ km s^{-1}. The z- and x-coordinates are in units of R_j. The contour lines are separated by a factor of 1.3, and the density scale covers the range from $\simeq 0.02$ up to $363/n_a$. The maximum density reached by the cold shell developed at the head of the jet is $n_{\text{sh}}/n_a(x_0) \approx 363, 294, 197, 69$, and 32 in (*a*)–(*e*), respectively.
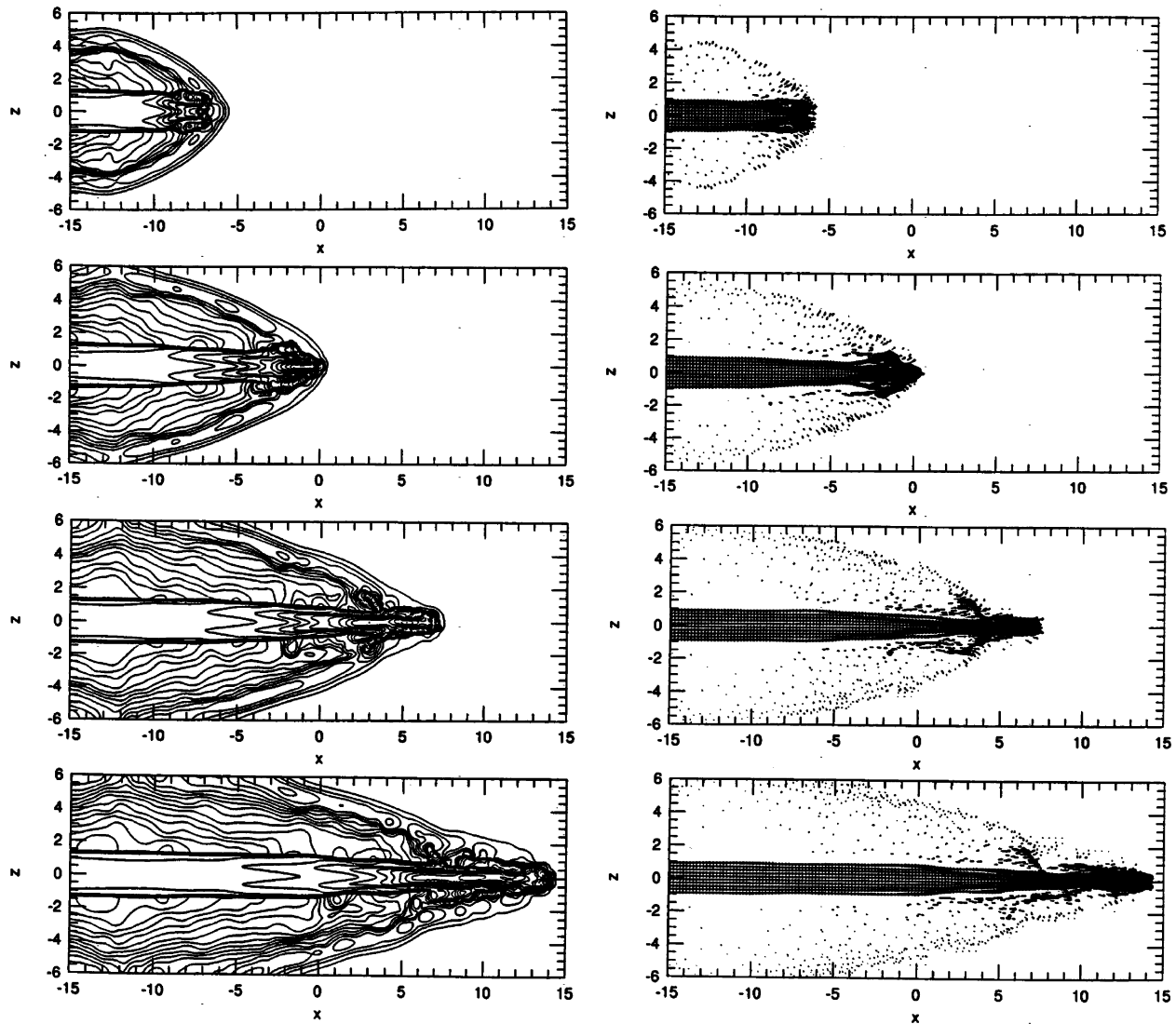
FIG. 2.—Same as Fig. 1, but for a radiative cooling jet propagating into a homogeneous ambient medium ($\alpha = 0$, $\beta = 0$). The initial conditions are the same as in Fig. 1. The contour lines are separated by a factor of 1.3, and the density scale covers the range from $\simeq 0.16$ up to $400/n_a$. The times (in units of $t_{ja} = R_j/c_a = 38.2$ yr) and jet head positions depicted are, from top to bottom, $0.70t_{ja}$ and $10.6R_j$; $1.05t_{ja}$ and $17.6R_j$; $1.40t_{ja}$ and $24.6R_j$; and $1.75t_{ja}$ and $31.6R_j$. The maximum density of the cold shell at the head, $n_{sh}/n_a(x_0)$, is $\approx 195, 400, 238$, and 272 from top to bottom, respectively.

fragmentation. No internal shocks are formed along the beam. For an ambient medium with negative density gradient (increasing η), the cooling length behind the bow shock (q_{bs}) increases as the jet propagates downstream (eqs. [4], [5]): q_{bs} increases from 8.1 at $t = 0$ to ~ 3958 at $t = 1.45t_{ja}$, so that the bow shock becomes more adiabatic as the beam propagates. By contrast, q_{js} initially decreases from 0.3 at $t = 0$ to ~ 0.1 at $t = 0.25t_{ja}$, in agreement with equation (6), then increases to ~ 149 at $t = 1.45t_{ja}$ (eq. [7]), so that the jet shock becomes less radiative.

For comparison, Figure 5 shows, from top to bottom, the midplane radiative emissivity [$L = n^2 \Lambda(t)$] contours of the jets of Figures 2, 3, and 4, respectively, when their working surfaces are at a position $x \simeq 25R_j$. In the decreasing-density ambient medium (Fig. 5, bottom), the jet is very faint with a maximum emissivity that is $\sim 1.3 \times 10^{-2}$ of that of the jet in the homogeneous ambient medium (Fig. 5, top). The latter, in turn, has a maximum emissivity that is $\sim 1.6 \times 10^{-2}$ of that of the jet in the increasing-density ambient medium (Fig. 5, center). The time evolution of the

radiative emissivity of the head of the jets of Figures 2, 3, and 4 in the axis ($y = z = 0$) is depicted in Figure 6. As the jet in the decreasing-density ambient medium ($\alpha = 0.5$, $\beta = -5/3$) propagates downstream, the emissivity (which is generally dominated by the jet-shocked material) decays, and the shock becomes mostly adiabatic. For the jet propagating into the homogeneous ambient medium ($\alpha = 0$, $\beta = 0$), the varying pattern of the emissivity is correlated with the density oscillations of the cold shell discussed above. The emissivity of the jet propagating into the increasing-density medium ($\alpha = 0.5$, $\beta = 5/3$) (which is initially dominated by the bow shock and, after $t \simeq 1.25t_{ja}$, by the internal knot closest to the head) increases with time, as expected.

3.2. Jets with Different Density Ratio Relative to the Ambient Medium

Figure 7 depicts the velocity distribution of the central slice of cooling jets with different η propagating into an $\alpha = 0.5$ ambient medium with positive ($\beta = 5/3$) density
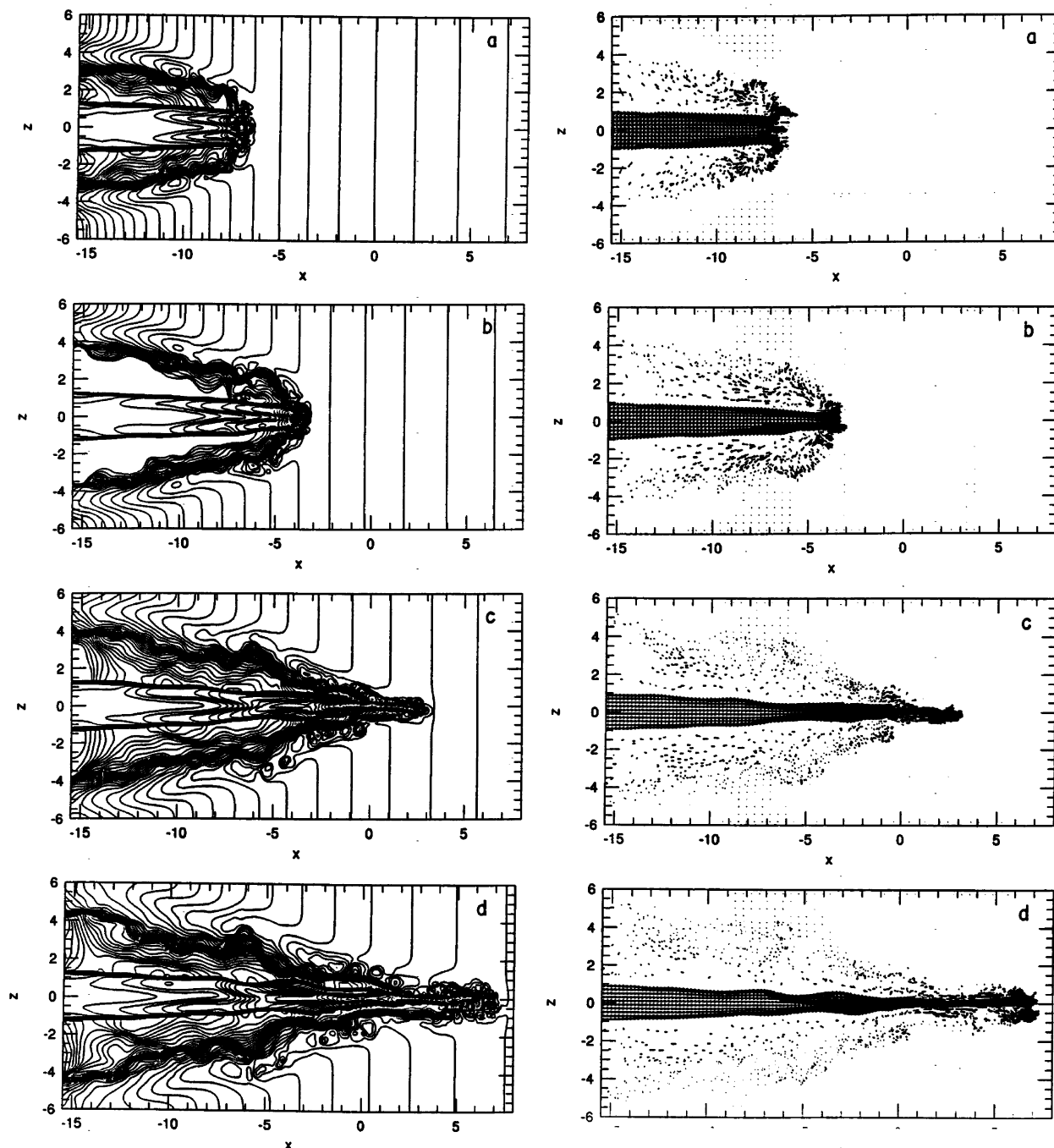
FIG. 3.—Same as Fig. 2, but for a radiative cooling jet propagating into an ambient medium with positive density (and pressure) gradient ($\alpha = 0.5$, $\beta = 5/3$). The initial conditions are the same as in Fig. 2. The contour lines are separated by a factor of 1.2, and the density scale covers the range from $\simeq 0.01$ up to $3550/n_a$. The times and jet head positions are (a) $0.85t_{ja}$ and $8.8R_j$, (b) $1.25t_{ja}$ and $12R_j$, (c) $1.65t_{ja}$ and $18.7R_j$, and (d) $1.96t_{ja}$ and $23R_j$.

(and pressure) stratification (see the corresponding density maps in Fig. 2 of GBB). The jets have, for $\eta = 1$, $q_{bs}(x_0) \approx$ 3.1 and $q_{js}(x_0) \approx 3.1$; for $\eta = 3$, $q_{bs}(x_0) \approx 8.1$ and $q_{js}(x_0) \approx$ 0.3; and for $\eta = 10$, $q_{bs}(x_0) \approx 16.7$ and $q_{js}(x_0) \approx 0.008$, and other initial conditions the same as in previous runs (Table 1). The $\eta = 1$ jet is the most evolved, reaching the end of the computational domain at $t = 1.85t_{ja}$, while the $\eta = 3$ jet reaches the end at $t = 1.65t_{ja}$ and the $\eta = 10$ jet at $t = 1.25t_{ja}$. The maximum density of the shells at the jet heads are $n_{sh}/n_a(x_0) \approx 211$, 638, and 2540, respectively. Jets with larger η are less affected by the increasing ambient density and pressure gradients and show less focusing by the compressing ambient medium. Consistently, the development of

the K-H modes (see also Fig. 3), which cause the beam pinching and wiggling, are stronger in small-η jets. The internal oblique shocks driven by beam pinching have a typical separation of a few jet radii, in agreement with the observed internal knots of young stellar object (YSO) jets (see, e.g., MRR). Like the $\eta = 3$ jet (see Fig. 3), both the $\eta = 1$ and $\eta = 10$ jets also show oscillatory propagation velocities due to the competing effects of the increasing ambient density and the ratio $\epsilon^{1/2}$ (eq. [3]). Tables 3 and 4 show the velocity variations in the heads of the $\eta = 1$ and 10 jets. In the case of the $\eta = 10$ jet, the velocity oscillations are smoother, and the smaller velocity variation in this case is not enough to cause significant fluctuations on the ambient
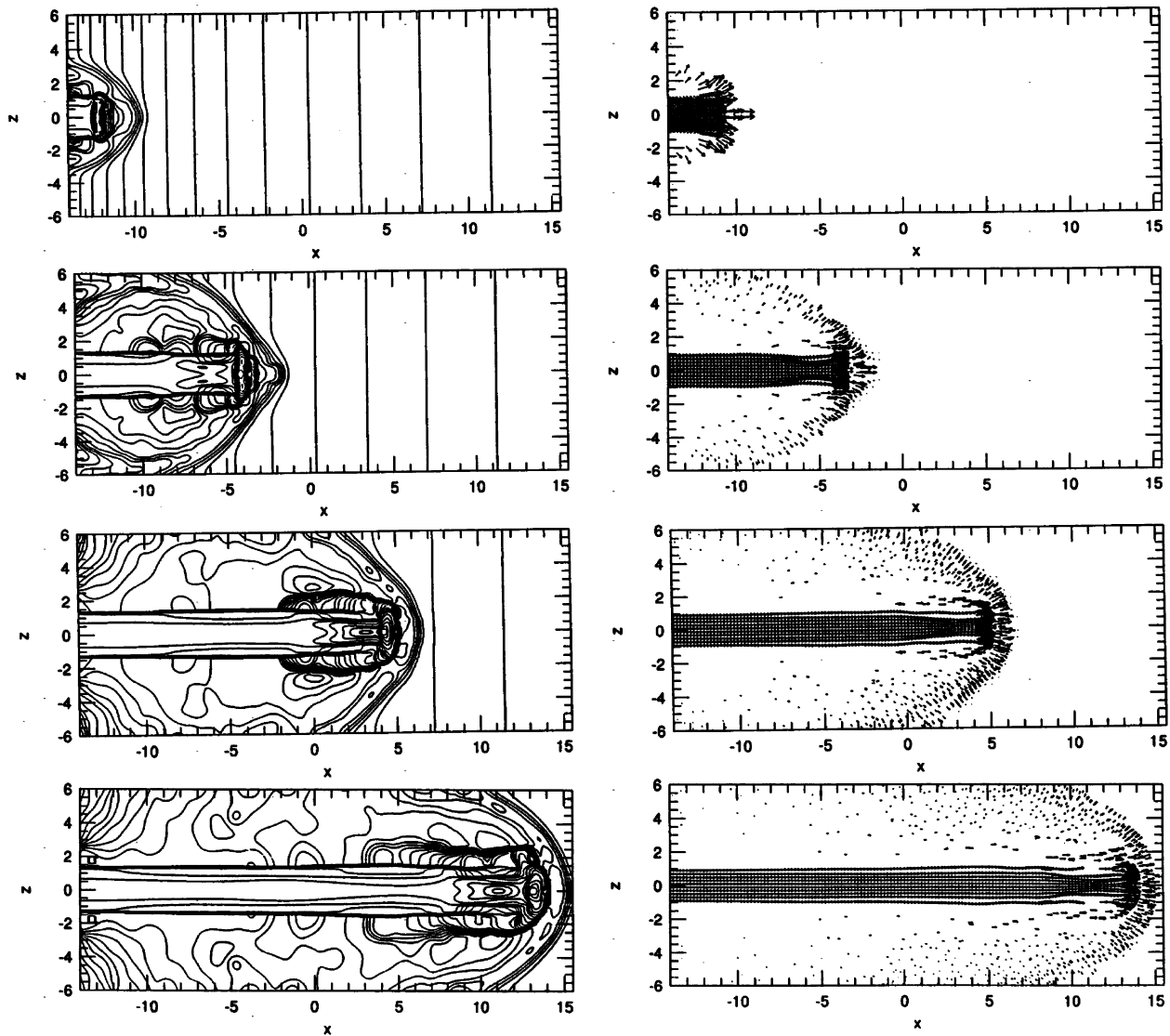
FIG. 4.—Same as Fig. 2, but for a radiative cooling jet propagating into an ambient medium with negative density (and pressure) gradient ($\alpha = 0.5$, $\beta = -5/3$). The initial conditions are the same as in Fig. 2. The contour lines are separated by a factor of 1.2, and the density scale covers the range from $\simeq 0.01$ up to $29/n_a$. The times and jet head positions are, from top to bottom, $0.25t_{ja}$ and $4.3R_j$; $0.65t_{ja}$ and $12.3R_j$; $1.05t_{ja}$ and $20.8R_j$; and $1.45t_{ja}$ and $30R_j$. The maximum density contrast in the thin shell at the head is $n_{sh}/n_a(x_0) \approx 13, 23, 31$, and 18 from top bottom, respectively.

ram pressure ($n_a v_{bs}^2$), which decreases with increasing distance. The internal shocks of Figures 7a and 7b travel downstream under a similar variable velocity pattern as the working surface.

Figure 8 shows that, later ($t = 2.05t_{ja}$), the knots close to

the head of the $\eta = 1$ jet break and *separate*, but this effect may have been amplified by the nearby continuous boundary.

Figure 9 depicts three cooling jets with different η propagating into an $\alpha = 0.5$ ambient medium with negative

TABLE 3

VELOCITY OSCILLATIONS IN THE HEAD OF THE $\eta = 1$ JET
PROPAGATING INTO AN ENVIRONMENT OF
INCREASING DENSITY[a]

t/t_{ja}	$(x_{bs} - x_0)/R_j$	$\epsilon^{1/2}$	v_{bs} (km s^{-1})	$n_a v_{bs}^2$ [b]
0	0	1	199	1.4×10^2
0.85	7.7	1.3	125	7.9×10^2
1.25	13.1	6	224	5.3×10^3
1.85	18.9	5	126	2.9×10^3

[a] As shown in Fig. 7a ($\alpha = 0.5$, $\beta = 5/3$).
[b] In units of $n_a(x_0)c_a^2 = 5.5 \times 10^{14}$ cm^{-1} s^{-2}.

TABLE 4

VELOCITY OSCILLATIONS IN THE HEAD OF THE $\eta = 10$ JET
PROPAGATING INTO AN ENVIRONMENT OF
INCREASING DENSITY[a]

t/t_{ja}	$(x_{bs} - x_0)/R_j$	$\epsilon^{1/2}$	v_{bs} (km s^{-1})	$n_a v_{bs}^2$ [b]
0	0	1	302	3.3×10^2
0.45	7.5	1.1	232	2.6×10^3
0.65	10.5	1.7	249	4.8×10^3
1.05	15.9	1.7	212	6.3×10^3
1.25	19	2	259	1.2×10^4

[a] As shown in Fig. 7c ($\alpha = 0.5$, $\beta = 5/3$).
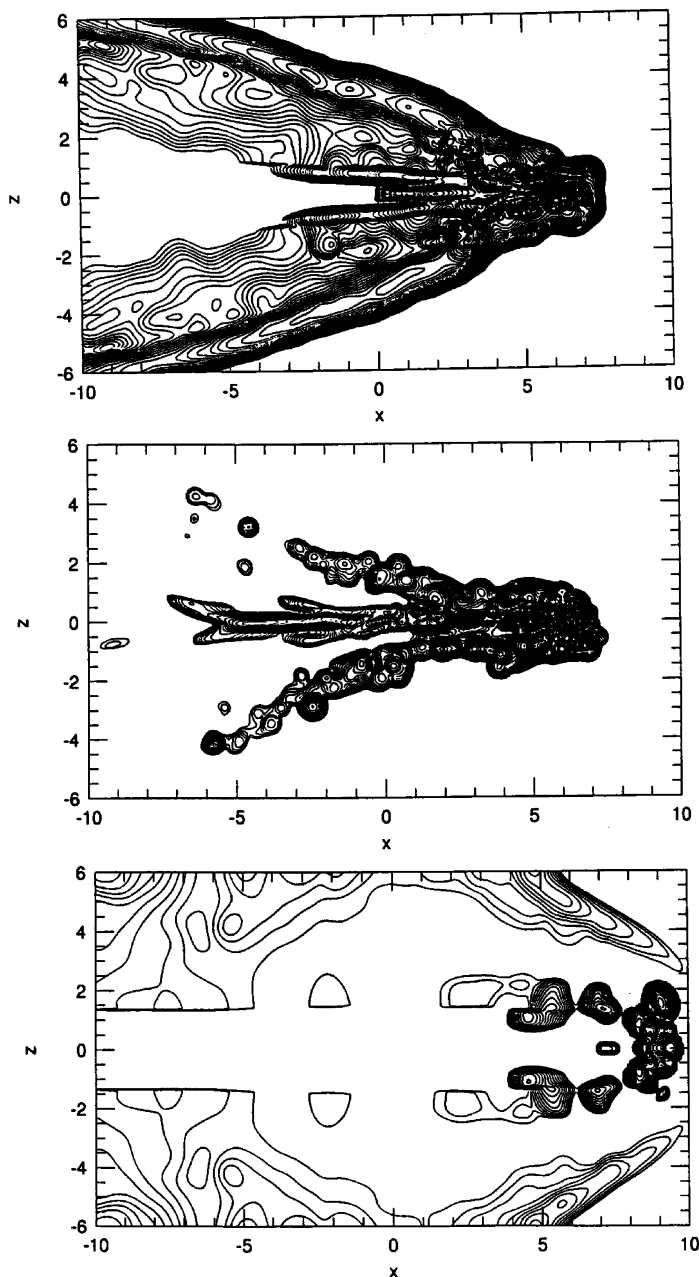[b] In units of $n_a(x_0)c_a^2 = 5.5 \times 10^{14}$ cm^{-1} s^{-2}.

FIG. 5.—Midplane radiative emissivity contour of the jets of Figs. 2, 3, and 4 when they reach $x \simeq 25R_j$. *Top*, jet in the homogeneous ambient medium ($\alpha = 0$, $\beta = 0$) at $t = 1.4t_{ja}$; *center*, jet in the increasing-density ambient medium ($\alpha = 0.5$, $\beta = 5/3$) at $t = 1.96t_{ja}$; *bottom*, jet in the decreasing-density ambient medium ($\alpha = 0.5$, $\beta = -5/3$) at $t = 1.25t_{ja}$. The emissivity is in units of 3.8×10^{-19} ergs cm^{-3} s^{-1}. The contour lines are separated by a factor of 1.2, and the emissivity scale covers the range from $\simeq 0.01$ up to 3.3×10^5 in code units.

($\beta = -5/3$) density (and pressure) stratification and the same initial conditions as Figure 7. As in Figure 4, in all cases the cocoon becomes broad and relaxed. The cold shell is thin, and its density is low (see Fig. 9), in qualitative agreement with equation (7). The beam decollimation is significantly larger for the smallest η jet.

3.3. Jets with Different $M_a = v_j/c_a$

Figure 10 depicts an $\eta = 3$ cooling jet propagating into an $\alpha = 0.5$ ambient medium with positive ($\beta = 5/3$) density
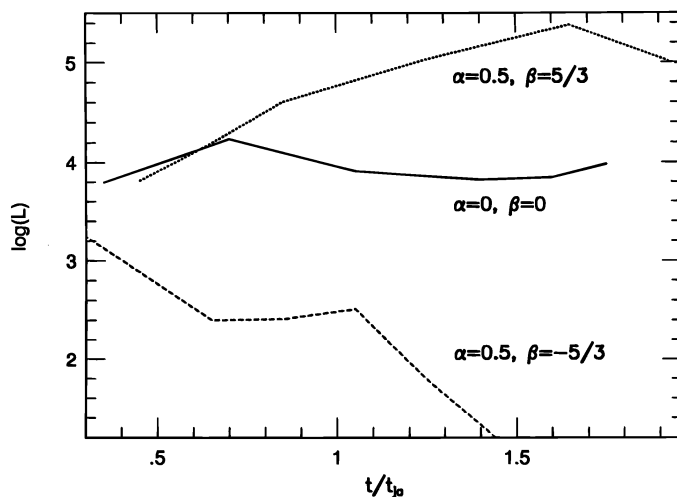

FIG. 6.—Time evolution of the axial radiative emissivity of the head of the jets of Figs. 2 ($\alpha = 0$, $\beta = 0$), 3 ($\alpha = 0.5$, $\beta = 5/3$), and 4 ($\alpha = 0.5$, $\beta = -5/3$). The emissivity is in units of 3.8×10^{-19} ergs cm^{-3} s^{-1}.

(and pressure) stratification and $M_a = 12$ (or $v_j = 199$ km s^{-1}), which can be compared with the jet of Figure 3 for which $M_a = 24$. The initial values of $q_{bs}(x_0) \approx 0.5$ (eq. [5]) and $q_{js}(x_0) \approx 1.9 \times 10^{-2}$ (eq. [7]) for $\eta = 3$ (Table 1) imply that both shocks initially cool very fast and that the jet shock is nearly isothermal (see, e.g., GB93). The jet reaches the end of the domain at $x = 20R_j$ at $t = 3.85t_{ja}$ (Fig. 10c). This snapshot can be compared with Figure 3c, in which the $M_a = 24$ jet has propagated about the same distance (at $t = 1.65t_{ja}$). The smaller M_a jet seems to be less affected by the focusing effect of the ambient medium with increasing pressure, but the interface with the cocoon is more affected by turbulent entrainment (CMGB).

Figure 11 depicts a jet propagating into an $\alpha = 0.5$ ambient medium with negative ($\beta = -5/3$) density (and pressure) stratification (compare this $M_a = 12$ jet with the $M_a = 24$ case in Fig. 4). The beam decollimation close to the head caused by the decreasing ambient pressure is slightly larger in the smaller, more evolved M_a jet. The maximum density in the cold shell at the jet head is also smaller in this latter case.

3.4. Adiabatic versus Radiative Cooling Jets

Figure 12 depicts the central density contours and velocity distribution of an adiabatic and a radiative cooling jet (as in Fig. 3), both with $\eta = 3$ and $M_a = 24$ propagating into an $\alpha = 0.5$ ambient medium with positive ($\beta = 5/3$) density (and pressure) stratification at $t = 1.45t_{ja}$. The ambient medium compresses the cooling jet more than the adiabatic jet, and the thinner, lower pressure cocoon around the cooling jet is less able to preserve its structure. The propagation velocities are very similar until $t \approx 1.45t_{ja}$, when, because of the larger focusing ($> \epsilon^{1/2}$) of the head, the radiative jet propagates about twice as fast. The maximum density behind the shock is $n_{sh}/n_a(x_0) \approx 650$ for the cooling jet and 6 for the adiabatic jet.

Figure 13 depicts the density contours and velocity distribution of an adiabatic and a radiative cooling jet (also in Fig. 4), both with $\eta = 3$ and $M_a = 24$ propagating into an $\alpha = 0.5$ ambient medium with negative ($\beta = 5/3$) density (and pressure) stratification, at $t = 0.85t_{ja}$ when they reach
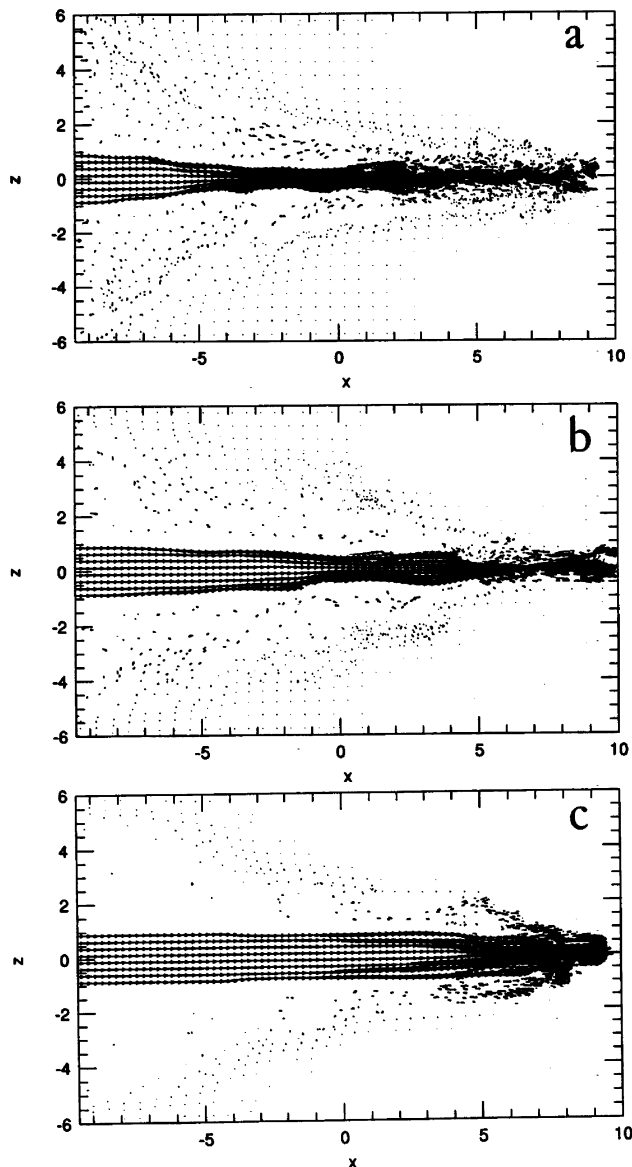
FIG. 7.—Velocity distribution of the midplane of cooling jets with different η propagating into an $\alpha = 0.5$ ambient medium with positive ($\beta = 5/3$) density (and pressure) stratification: (a) $\eta = 1$; (b) $\eta = 3$; (c) $\eta = 10$. The corresponding density contours are shown in Fig. 2 of GBB. The other initial conditions are the same as in the previous figures. The $\eta = 1$ jet reaches the end of the computation domain at $t = 1.85t_{\mathrm{ja}}$; the $\eta = 3$, at $t = 1.65t_{\mathrm{ja}}$; and the $\eta = 10$, at $t = 1.25t_{\mathrm{ja}}$.

FIG. 8.—Midplane density contours (top) and the corresponding velocity distribution (bottom) of the $\eta = 1$ jet of Fig. 7 at $t = 2.05t_{\mathrm{ja}}$. The contour lines are separated by a factor of 1.3, and the density scale covers the range from $\simeq 0.05$ up to $205/n_a$. The knots close to the head seem to break and separate apart.

$x \approx 20R_j$. The propagation velocity v_{bs}, the decreasing ambient ram pressure, and the head decollimation are very similar in both jets, although slightly larger in the adiabatic case. The density behind the shock is $n_{\mathrm{sh}}/n_a(x_0) \approx 32$ for the cooling jet and 6 for the adiabatic jet.

4. DISCUSSION AND CONCLUSIONS

In this work, we have presented fully three-dimensional hydrodynamic simulations of initially overdense, radiative cooling jets propagating into stratified isothermal ambient media with a power-law density and pressure distribution (eq. [1]). We also have investigated the behavior of adiabatic jets propagating into similar stratified environments. As in our previous work (GB93, GB94; CMGB; GBB), the
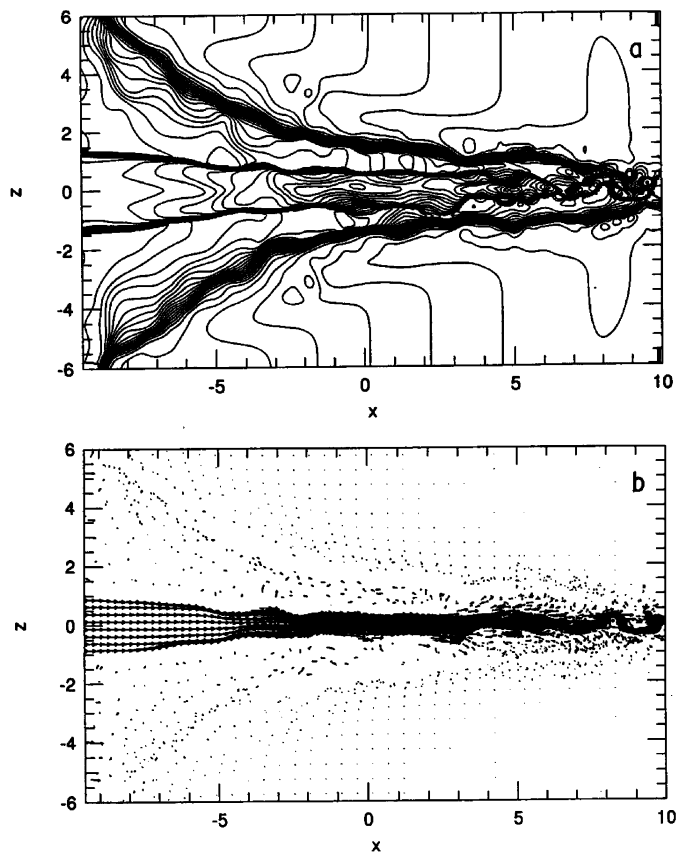
simplified treatment of the radiative cooling of the gas prevents us from performing a detailed comparison of our models with the radiation from observed protostellar jets. In particular, the density contour maps, while describing reasonably well the expected gas distribution, do not necessarily correspond to the observed emission-line images. Nonetheless, with the help of those maps, we can delineate some basic structural characteristics and dynamics and compare with observed protostellar jets.

Our results show that jets propagating into regions of an ambient medium with negative density (pressure) gradient develop a broad and relaxed cocoon and suffer beam decollimation at the head. Their propagation velocity increases, on average, as they propagate downstream because of the drop of the ambient density and ram pressure. The beam decollimation is larger for the small-η jets, as their momentum flux is smaller (Figs. 4 and 7). No internal knots are formed in these cases, and the weak radiative shocks at the head provide little radiation. This suggests a possible explanation for the invisible portions of the observed outflows, as we have proposed in GBB. For example, the observed gaps close to the source of Haro 6-5B (or FS Tau B), AS 353, or 1548 C27 jets (e.g., MRR; Hartigan, Mundt, & Stocke 1986; Mundt et al. 1984, 1987), or the gaps between the beam and the distant bow shock (e.g., Haro 6-5B), could be a product of such an effect (see also GBB).
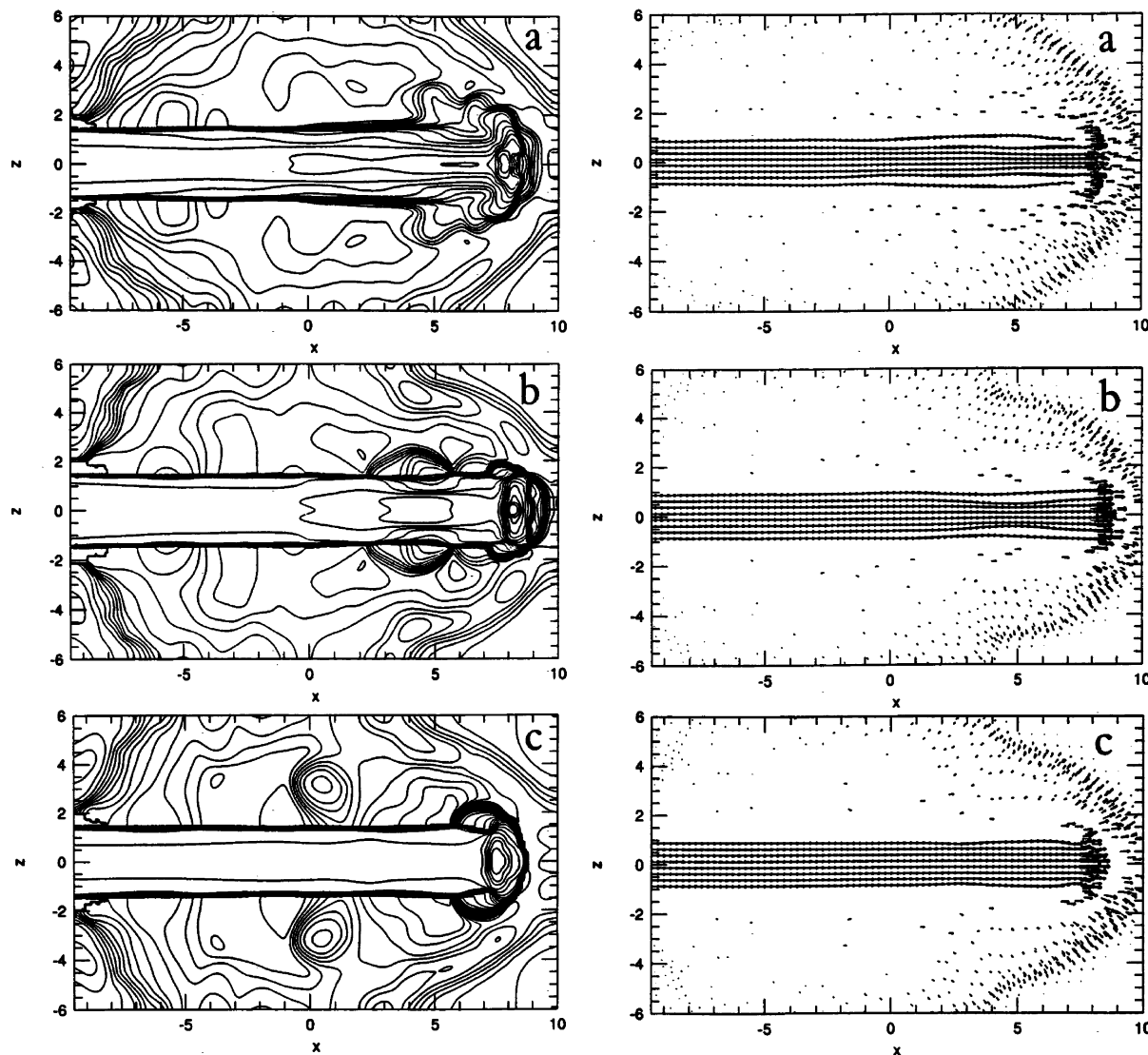
FIG. 9.—Midplane density contours (*left*) and the corresponding velocity distribution (*right*) of cooling jets with different η propagating into an $\alpha = 0.5$ ambient medium with negative ($\beta = -5/3$) density (and pressure) stratification and the same initial conditions as Fig. 5: (*a*) $\eta = 1$; (*b*) $\eta = 3$; (*c*) $\eta = 10$. The jets reach the end of the domain, at $x \approx 20R_j$, at $t = 1.05t_{ja}$ ($\eta = 1$), $0.95t_{ja}$ ($\eta = 3$), and $0.85t_{ja}$ ($\eta = 10$) in (*a*)–(*c*), respectively. The contour lines are separated by a factor of 1.3, and the density scale covers the range from $\simeq 0.01$ up to $58/n_a$. The maximum density in the cold shell at the head is $n_{sh}/n_a(x_0) \approx 4.4$, 33, and 58, respectively.

Jets propagating into an ambient medium with increasing density (pressure) have their cocoon/shroud compressed and pushed backward by the ambient ram pressure, and the beam is highly collimated. The compressing medium promotes beam focusing and wiggling and the formation of traveling internal shocks via beam pinching. The bow shock–like structure at the head disappears. Jets with larger η are less focused by the compressing medium, as a consequence of their larger momentum flux. We found that, within $\sim 30R_j$ an $M_a = 24$ ($v_j \approx 398$ km s^{-1}) jet with $\eta \leq 3$, propagating into a positive density gradient medium, wiggles and develops regularly spaced traveling knots close to the head (see also GBB).

Protostellar jets are generally well collimated and knotty and often show one or more bow shock features at the head (see, e.g., Reipurth 1989a; Hartigan, Raymond, & Meaburn 1990). A number of authors (e.g., Hartigan & Raymond 1992; Kofman & Raga 1992; Raga & Kofman 1992; SN;

GB94) have shown that the internal traveling bright knots may be produced by small-period variations in the velocity of jet ejection. This mechanism favors the formation of knots closer to the driving source that become fainter and disappear at larger distances, as, for example, in jet systems like HH 34 and HH 111 (see, e.g., Reipurth 1989b). On the other hand, BFK and GB93 have shown that, as a result of radiative cooling, K-H instabilities were less effective at driving internal shocks in beams propagating into a *homogeneous* ambient medium. In the present work, however, we find that propagation of a radiative cooling jet into an ambient medium of increasing density (pressure) may drive the formation of internal knots close to the jet head. This seems to be the case, for example, for the Haro 6-5B northern and HH 24G jets (Mundt et al. 1990; MRR), which present an elongated wiggling and knotty structure far from the source, very similar to those of Figures 3 and 7 (see GBB for a detailed discussion).
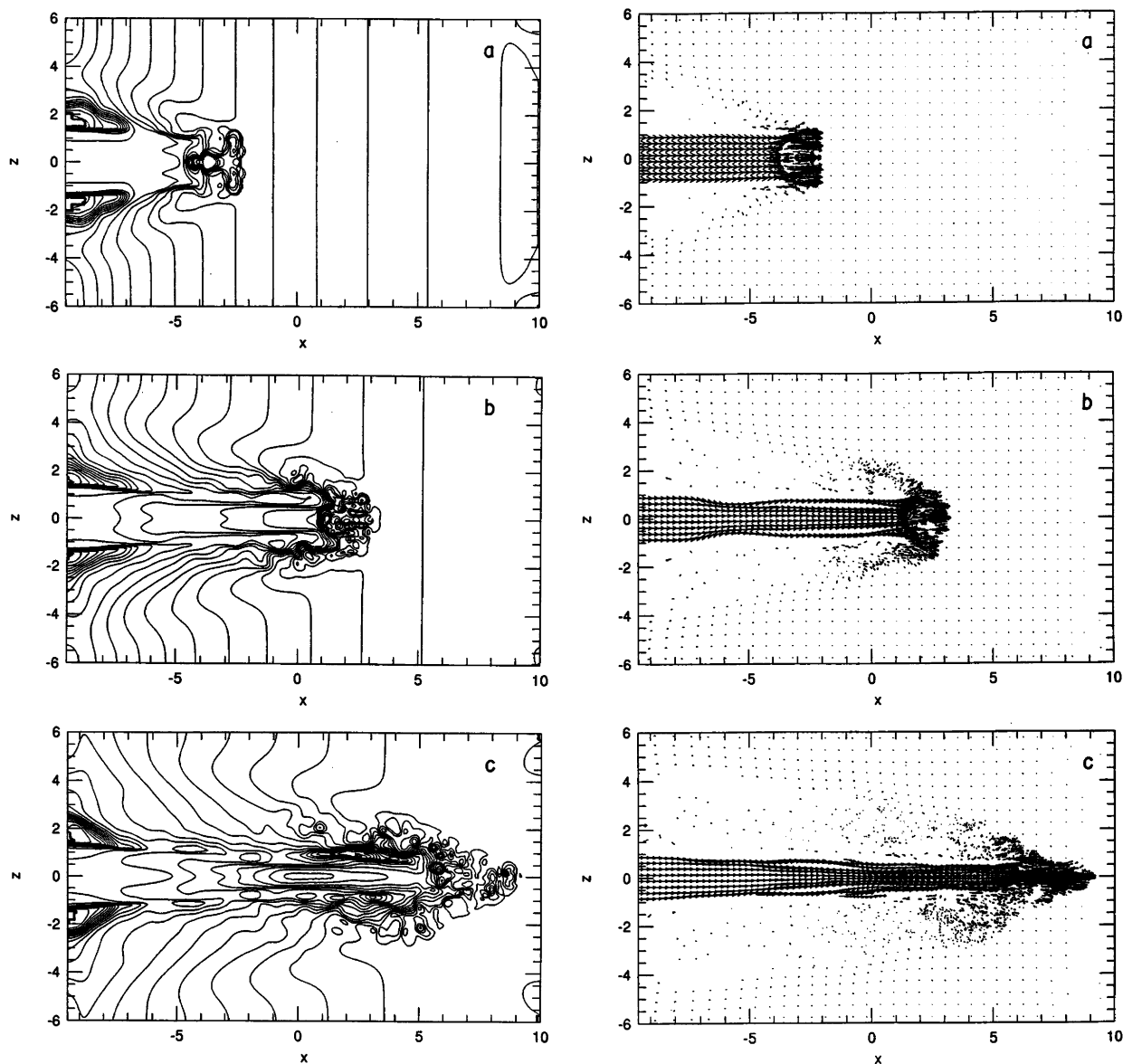
FIG. 10.—Same as Fig. 9, but for an $\eta = 3$ cooling jet propagating into an $\alpha = 0.5$ ambient medium with positive ($\beta = 5/3$) density (and pressure) stratification and $M_a = 12$ (or $v_j = 199$ km s^{-1}). The other initial conditions are the same as in Fig. 3, except that $q_{bs}(x_0) \approx 0.5$ (eq. [5]) and $q_{js}(x_0) \approx 1.9 \times 10^{-2}$. The contour lines are separated by a factor of 1.3, and the density scale covers the range from $\simeq 0.01$ up to $284/n_a$. The times depicted are (a) $1.15t_{ja}$, (b) $2.45t_{ja}$, and (c) $3.85t_{ja}$.

Large amplitude side-to-side wiggles and knots are also observed in the HH 83, HH 84, HH 85, HH 110 (e.g., Reipurth 1989a, 1989b), and HH 30 jets (Mundt et al. 1990; MRR), all of which are immersed in complex regions. The HH 30 jet, for example, belongs to the HL Tau/HH 30 region, which shows five outflows and a number of reflection nebulae associated with YSOs. As for the Haro 6-5B jet, we suggest that the observed collimated, wiggling, and knotty structure of these jets could be due to K-H instabilities driven by a compressing medium of increasing density (as in Figs. 3 and 7). An alternative, recently discussed by Raga, Cantó, & Biro (1993), is that the jet is ejected from a precessing source into a homogeneous ambient medium.

In addition, our results indicate that increasing-density environments destroy the bow shock at the head. Some authors have demonstrated that bow shocks can be formed

in jets with continuous ejection (e.g., Norman et al. 1982; BFK; GB93) or with multiple outflow episodes of long period (e.g., Hartigan & Raymond 1992; Raga & Kofman 1992; SN; GB94) and can keep their structure stable in portions of the jet where the ambient medium is more *homogeneous* (GB93). However, there are cases that show no evidence of a terminal bow shock feature (e.g., some sources of the MRR sample), which may match some of our results (Figs. 3, 7, and 8). There are other cases, e.g., the Haro 6-5B (MRR) and HH 30 jets (López et al. 1995), in which the elongated beam is separated by a long gap from the distant bow shock. The bow shock in these cases could be a relic of an earlier outflow episode or the place where the jet impacts a dense portion of the ambient medium after a long expansion through a decreasing-density (pressure) medium (see GBB).

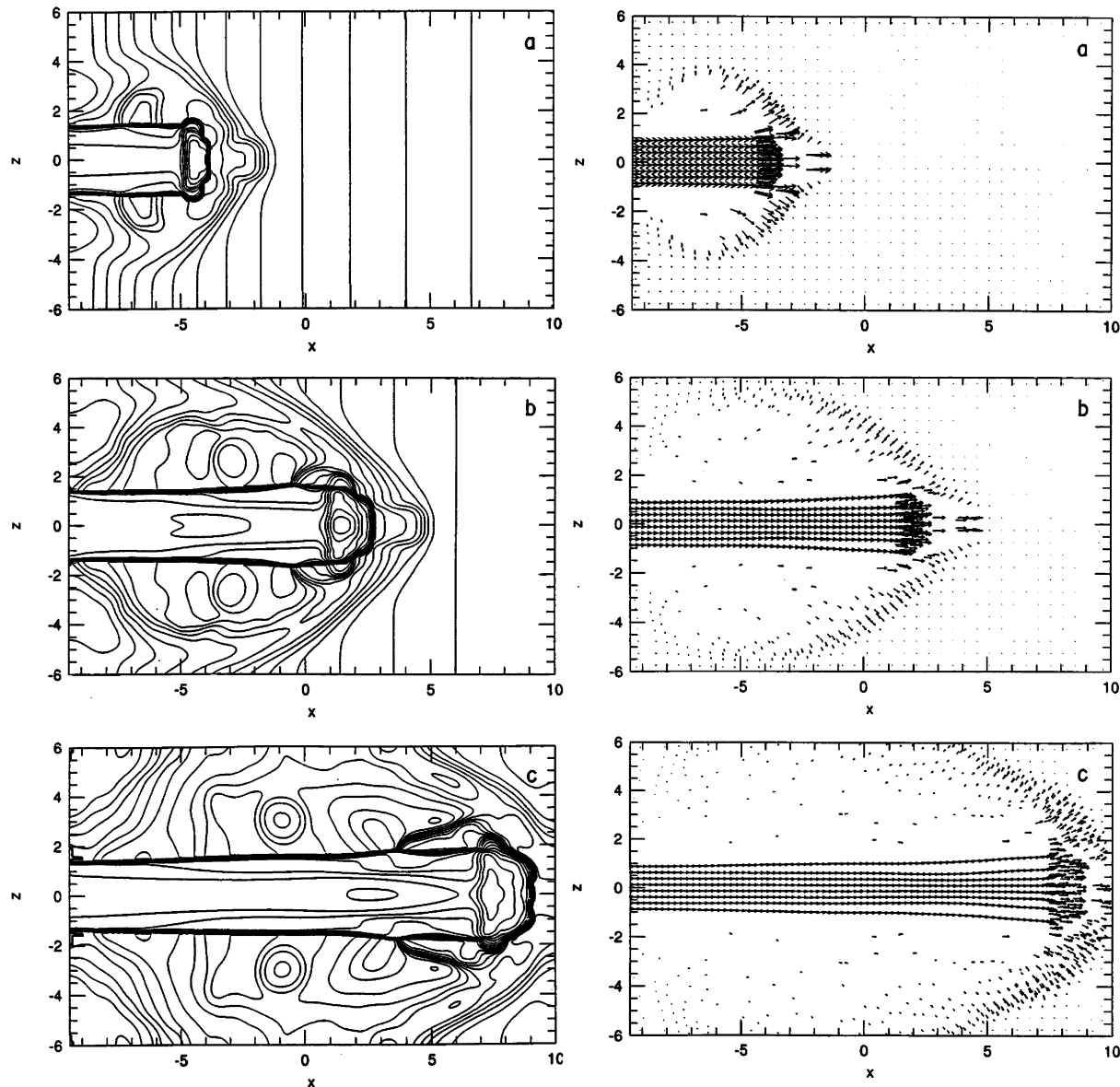Although, on average, the jets propagating into an

FIG. 11.—Same as Fig. 10, but for an $\alpha = 0.5$ ambient medium with negative ($\beta = 5/3$) density (and pressure) stratification and $M_a = 12$ (or $v_j = 199$ km s^{-1}). The other initial conditions are the same as in Fig. 4, except that $q_{bs}(x_0) \approx 0.5$ (eq. [5]) and $q_{js}(x_0) \approx 1.9 \times 10^{-2}$. The contour lines are separated by a factor of 1.3, and the density scale covers the range from $\simeq 0.01$ up to $14/n_a$. The times depicted are (a) $0.65t_{ja}$, (b) $1.25t_{ja}$, and (c) $1.85t_{ja}$. The jet reaches the end of the domain at $x \approx 20R_j$. The maximum density in the cold shell is $n_{sh}/n_a(x_0) \approx 14, 11$, and 6 in (a)–(c), respectively.

increasing (decreasing) density environment are decelerated (accelerated) by the increasing (decreasing) ram pressure of the ambient medium, we find that their propagation velocities v_{bs} have an oscillatory pattern due to the competing effects between the varying density ratio η and the ratio of jet to head radius $\epsilon^{1/2} = R_j/R_h$. The internal traveling shocks that develop in jets propagating into positive density gradient environments (Figs. 3, 7, and 8) also follow a variable velocity pattern, with their speeds becoming closer to v_{bs} as they approach the jet head. This is in qualitative agreement with recent measurements of the tangential velocity of the knots of Haro 6-5B (Eislöffel 1993). Variations of the shock velocity must be accompanied by variations in the intensity of emission from cooling regions behind the shocks. Thus further detections of intensity and knot proper-motion variability in other systems would provide a possible check of our predictions.

In the comparison of jets with different initial Mach numbers M_a propagating into ambient portions of increasing density, we find that (Figs. 3 and 10) the smaller M_a jet ($M_a = 12$) seems to be less affected by the focusing effect of the ambient medium with increasing pressure. Because of its smaller pressure cocoon, the interface between the cocoon and the smaller M_a jet is more affected by lateral turbulent entrainment (see, e.g., Raga, Cabrit & Cantó 1995; de Gouveia Dal Pino 1995). In a recent investigation of radiative cooling jets propagating into *homogeneous* ambient media (CMGB), we found that the lateral entrainment of ambient gas through turbulent mixing at the contact discontinuity is relevant only for low Mach number ($M_j = M_a\eta^{1/2} \leq 3$), low density ratio ($\eta \leq 3$) flows, which, in general, are not appropriate for protostellar jets, for which $10 < M_j < 40$ and $\eta > 1$. Entrainment of ambient gas seems to be mostly through the bow shock in protostellar
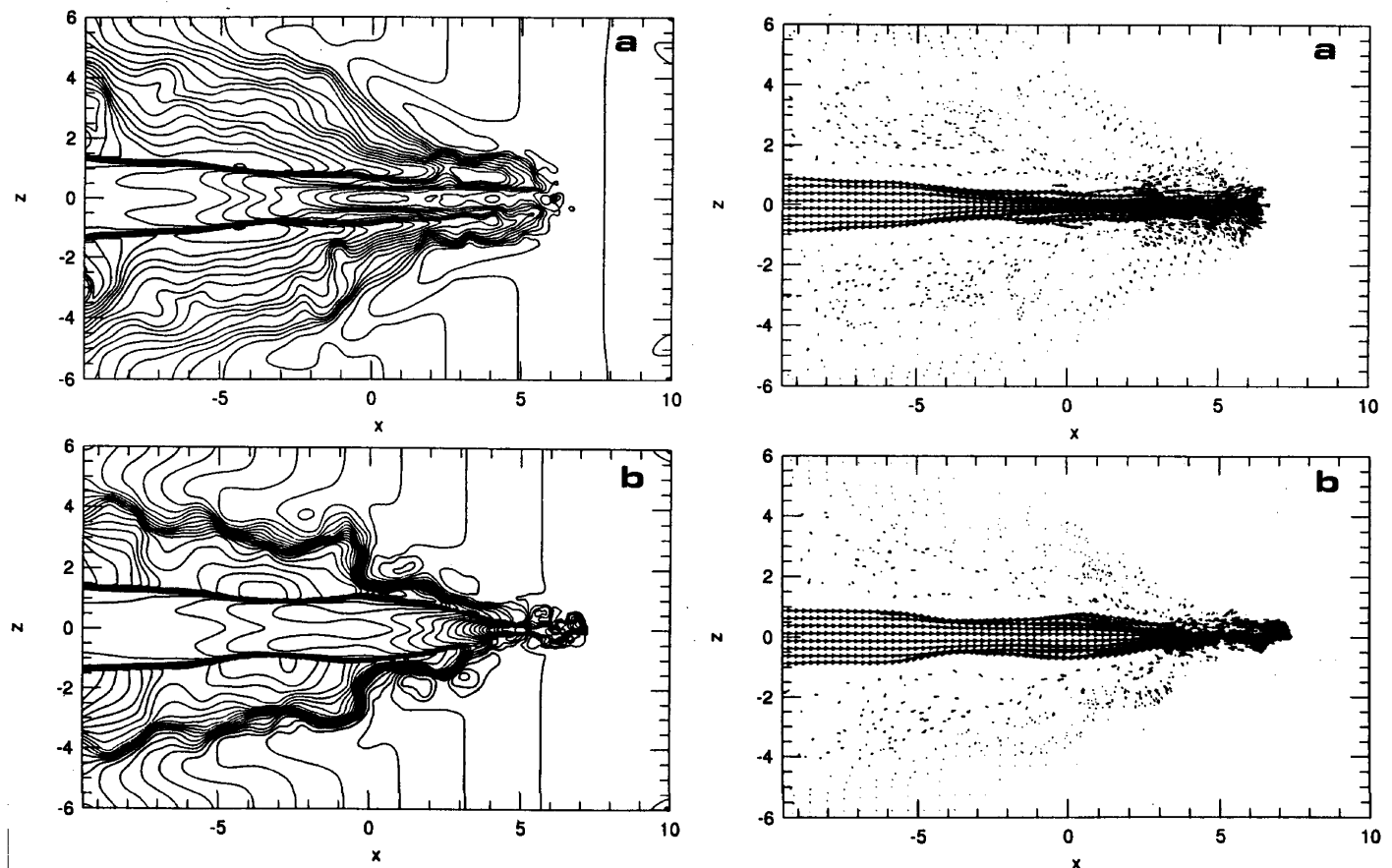
Fig. 12.—Central density contours (*left*) and velocity distribution (*right*) of (*a*) an adiabatic and (*b*) a radiative cooling jet, both with $\eta = 3$ and $M_a = 24$ propagating into an $\alpha = 0.5$ ambient medium with positive ($\beta = 5/3$) density (and pressure) stratification at $t = 1.45t_{ja}$. The contour lines are separated by a factor of 1.3, and the density scale covers the range from $\simeq 0.01$ up to $650/n_a$.
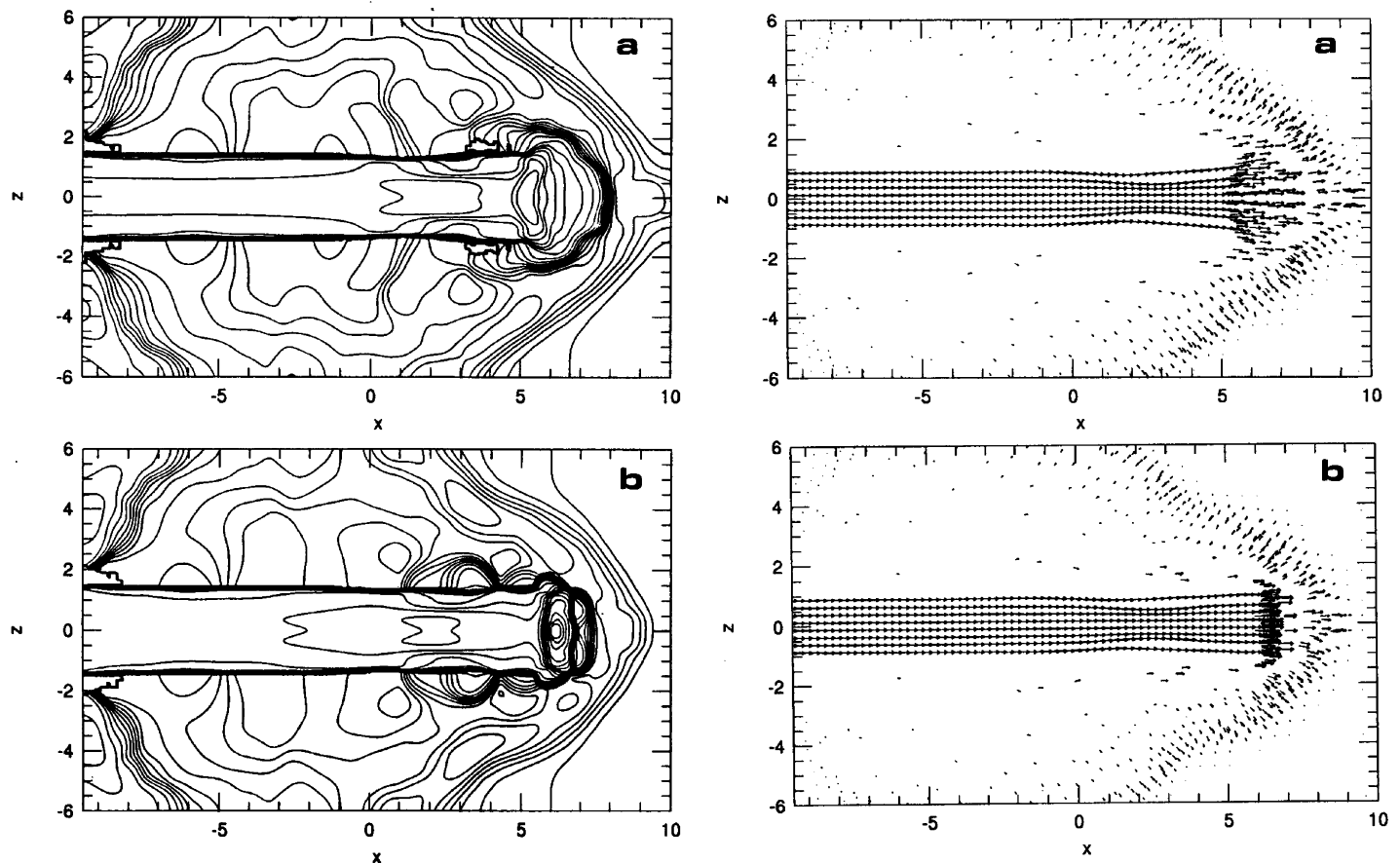

Fig. 13.—Same as Fig. 12, but for ambient medium with negative ($\beta = -5/3$) density (and pressure) stratification at $t = 0.85t_{ja}$, when the jets reach $x \approx 20R_j$. The contour lines are separated by a factor of 1.3, and the density scale covers the range from $\simeq 0.01$ up to $32/n_a$.

© **American Astronomical Society** • **Provided by the NASA Astrophysics Data System**

jets (CMGB). These results have ruled out models that propose that the molecular outflows associated with protostellar jets are produced predominantly through turbulent entrainment (e.g., Stahler 1993). In the present study, however, we find that jets with $M_j = 21$ (or $M_a = 12$ and $\eta = 3$) in an ambient medium of increasing density suffer considerable entrainment along the beam. This result suggests that, even in high Mach number jets, turbulent entrainment may play an important role in driving molecular outflows *if* the ambient medium has regions of varying density (and pressure). We note that the large line broadening (FWHM $\simeq$ 100–150 km s^{-1}) detected along portions of some of the jets of HL Tau/HH 30 complex (Mundt et al. 1990) is an indication that turbulent entrainment may be relevant in those regions, as suggested by Mundt et al.

We also performed short-time runs of adiabatic jets into stratified environments in order to compare their structure with that of radiative cooling jets (Figs. 12 and 13). In general, the radiative cooling jet propagating into an ambient medium of positive density gradient is more collimated by the compressing medium than the adiabatic jet. On the other hand, the adiabatic jet propagating into an ambient medium of negative density gradient suffers more head decollimation. Both effects are due to the fact that the adiabatic jet has a higher pressure cocoon, which is better able to preserve the beam structure in the compressing environment and to accelerate the ambient gas where its density is decreasing.

Finally, as in our previous investigations (GB93, GB94;

CMGB; GBB), in this study we have assumed a history-independent, optically thin radiative cooling function to compute the losses of a fully ionized flow. By not following the history-dependent effects of nonequilibrium ionization of the gas or the transfer of ionizing radiation, we have possibly underestimated the cooling rate in some parts of the postshock regions by as much as an order of magnitude (see, e.g., Innes et al. 1987). The inclusion of a detailed cooling evaluation, as in the one-dimensional calculations of Hartigan & Raymond (1992), would require a substantial increase in computer power. Although future work should take into account those effects, we expect that the gross dynamical features obtained in the present analysis will not change. This expectation is supported by the comparison of our results (see GB93, GB94) with the calculations of SN (see also their recent calculations for steady flows; Stone & Norman 1993a, 1994b), which included a nonequilibrium time-dependent cooling.

REFERENCES

Bally, J., & Devine, D. 1994, ApJ, 428, L65
Benz, W. 1990, in The Numerical Modelling of Stellar Pulsations, ed. J. R. Buchler (NATO ASI Ser. C, 302) (Dordrecht: Kluwer), 269
Birkinshaw, M. 1991, in Beams and Jets in Astrophysics, ed. P. A. Hughes (Cambridge: Cambridge Univ. Press), 278
Biro, S., & Raga, A. C. 1994, ApJ, 434, 221
Blondin, J. M., Fryxell, B. A., & Königl, A. 1990, ApJ, 360, 370 (BFK)
Chernin, L., Masson, C., de Gouveia Dal Pino, E. M., & Benz, W. 1994, ApJ, 426, 204 (CMGB)
de Gouveia Dal Pino, E. M. 1995, in AIP Conf. Proc. 345, ICPP 1994: International Conference on Plasma Physics, ed. P. Sakanaka & M. Tendler (Woodbury, NY: AIP), 427
de Gouveia Dal Pino, E. M., & Benz, W. 1993, ApJ, 410, 686 (GB93)
———. 1994, ApJ, 435, 261 (GB94)
de Gouveia Dal Pino, E. M., Birkinshaw, M., & Benz, W. 1996, ApJ, 460, L111 (GBB)
Eislöffel, J. 1993, Ph.D. thesis, Univ. Heidelberg
Falle, S. A. E. G., & Raga, A. C. 1993, MNRAS, 261, 573
Falle, S. A. E. G., & Wilson, M. J. 1985a, MNRAS, 216, 79
———. 1985b, MNRAS, 216, 971
Fuller, G. A., & Myers, P. C. 1992, ApJ, 384, 523
Hardee, P. E., White, R. E., III, Norman, M. L., Cooper, M. A., & Clarke, D. A. 1992, ApJ, 387, 460
Hartigan, P., Mundt, R., & Stocke, J. 1986, AJ, 91, 1357
Hartigan, P., & Raymond, J. 1992, ApJ, 409, 705
Hartigan, P., Raymond, J., & Meaburn, J. 1990, ApJ, 362, 624
Innes, D. E., Giddings, J. R., & Falle, S. A. E. G. 1987, MNRAS, 226, 67
Katz, J. 1989, Ph.D. thesis, Princeton Univ.
Kofman, L., & Raga, A. C. 1992, ApJ, 390, 359
López, R., Raga, A., Riera, A., Anglada, G., & Estalella, R. 1995, MNRAS, 274, L19

Morse, J. A., Hartigan, P., Cecil, G., Raymond, J. C., & Heathcote, S. 1992, ApJ, 399, 231
Mundt, R., Brügel, E. W., & Bührke, T. 1987, ApJ, 319, 275
Mundt, R., Bührke, T., Fried, J. W., Neckel, T., Sarcander, M., & Stocke, J. 1984, A&A, 140, 17
Mundt, R., Bührke, T., Solf, J., Ray, T. P., & Raga, A. C. 1990, A&A, 232, 37
Mundt, R., Ray, T. P., & Raga, A. C. 1991, A&A, 252, 740 (MRR)
Norman, M. L., Winkler, K.-H. A., Smarr, L., & Smith, M. D. 1982, A&A, 113, 285
Raga, A. C. 1993, Ap&SS, 208, 163
Raga, A. C., Binette, L., Cantó, J., & Calvet, N. 1990, ApJ, 364, 601
Raga, A. C., Cabrit, S., & Cantó, J. 1995, MNRAS, 273, 422
Raga, A. C., Cantó, J., & Biro, S. 1993, MNRAS, 260, 163
Raga, A. C., & Kofman, L. 1992, ApJ, 386, 222
Raga, A. C., & Noriega-Crespo, A. 1993, Rev. Mexicana Astron. Astrofis., 25, 149
Reipurth, B. 1989a, A&A, 220, 249
———. 1989b, in ESO Workshop on Low Mass Star Formation and Pre–Main Sequence Objects, ed. B. Reipurth (Garching: ESO), 247
Reipurth, B., Raga, A. C., & Heathcote, S. 1992, ApJ, 392, 145
Sanders, R. H. 1983, ApJ, 266, 73
Stahler, S. 1993, in Astrophysical Jets, ed. M. Livio, C. O'Dea, & D. Burgarella (Cambridge: Cambridge Univ. Press), 183
Stone, J. M., & Norman, M. L. 1993a, ApJ, 413, 198
———. 1993b, ApJ, 413, 210 (SN)
———. 1994a, ApJ, 420, 237
———. 1994b, ApJ, 422, 348
Wiita, P. J., Rosen, A., & Norman, M. L. 1990, ApJ, 350, 545